Pharmaceutical Research, Vol. 26, No. 10, October 2009 (© 2009)
DOI: 10.1007/s11095-009-9951-x

Research Paper

Characterization of a Microsphere Formulation Containing Glucose Oxidase and its *In Vivo* Efficacy in a Murine Solid Tumor Model

Qun Liu,[1] Andrew Michael Rauth,[2] Jiang Liu,[2] Karlo Babakhanian,[1] Xinyue Wang,[1] Reina Bendayan,[1] and Xiao Yu Wu[1,3]

Received May 31, 2009; accepted July 30, 2009; published online August 15, 2009

Purpose. This work focused on the characterization and *in vitro*/*in vivo* evaluation of an alginate/chitosan microsphere (ACMS) formulation of glucose oxidase (GOX) for the locoregional delivery of reactive oxygen species for the treatment of solid tumors.
Methods. The GOX distribution and ACMS composition were determined by confocal laser scanning microscopy and X-ray photoelectron spectroscopy. The mechanism of GOX loading and GOX-polymer interactions were examined with Fourier transform infrared spectroscopy and differential scanning calorimetry. *In vitro* cytotoxicity and *in vivo* efficacy of GOX-encapsulated ACMS (ACMS-GOX) were evaluated in EMT6 breast cancer cells and solid tumors.
Results. GOX was loaded into calcium alginate (CaAlg) gel beads *via* electrostatic interaction and the CaAlg-GOX-chitosan complexation likely stabilized GOX. Higher concentrations of GOX near the surface of ACMS were detected. GOX retained its integrity upon adsorption to CaAlg gel beads during the coating and after release from ACMS. ACMS-GOX exhibited cytotoxicity to the breast cancer cells *in vitro* and their efficacy increased with increasing incubation time. Intratumorally delivered ACMS-GOX significantly delayed tumor growth with much lower general toxicity than free GOX.
Conclusion. The results suggest that the ACMS-GOX formulation has the potential for the intratumoral delivery of therapeutic proteins to treat solid tumors.

KEY WORDS: antitumor activity; glucose oxidase; intratumoral delivery; microspheres; reactive oxygen species.

INTRODUCTION

Reactive oxygen species (ROS), including superoxide anion ($O_2^{\cdot -}$), hydrogen peroxide (H_2O_2) and hydroxyl radical (HO·), are byproducts of normal cellular metabolism which directly affect cellular functions, e.g. development, growth and aging. While a moderate level of intracellular ROS is essential to maintain appropriate redox balance and to stimulate cellular proliferation, high levels of ROS can result in detrimental damage to cells, including lipid peroxidation, protein oxidation and DNA damage, and ultimately cell death *via* apoptosis or necrosis (1–5). In fact some anticancer agents increase intracellular ROS level as one of the mechanisms of killing cancer cells, e.g. doxorubicin, daunorubicin (6,7), bortezomib (8) and 2-methoxyestradiol (9). Although many chemotherapeutic agents have been developed, the efficacy of traditional cancer chemotherapy is still unsatisfactory due to lack of selectivity for cancer *versus* normal cells, development of multidrug resistance (MDR) phenotypes in cancer cells, and insufficient local drug concentrations in tumors.

Strategies are sought to improve therapeutic selectivity based on differences between the cancer cells and normal cells. Ideally, such strategies will selectively kill cancer cells, overcome or bypass MDR, increase the local drug concentration, and elicit extended effects. Elevated oxidative stress, such as enhanced ROS generation, increased accumulation of ROS-mediated products and overexpression of antioxidant enzymes, has been found in cancer cells as compared to normal cells (10). These findings suggest that introduction of additional ROS concentration might allow selective killing of cancer cells *versus* normal cells. Owing to the short half-life of ROS, ROS-generating enzymes, e.g. glucose oxidase (GOX), have been investigated for treatment of tumors (11,12).

[1] Leslie Dan Faculty of Pharmacy, University of Toronto, 144 College Street, Toronto, Ontario M5S 3M2, Canada.
[2] Division of Experimental Therapeutics, Ontario Cancer Institute, Toronto, Ontario M5G 2M9, Canada.
[3] To whom correspondence should be addressed. (e-mail: xywu@phm.utoronto.ca)

ABBREVIATIONS: ACMS, Alginate/chitosan microspheres; ACMS-GOX, GOX encapsulated in alginate/chitosan microspheres; CaAlg, Calcium alginate; CLSM, Confocal laser scanning microscope; DD, Degree of deacetylation; DDI, Distilled and deionized; DSC, Differential scanning calorimetry; FBS, Fetal bovine serum; FITC, Fluorescein isothiocyanate; FR-GOX, Free glucose oxidase; FT-IR, Fourier transform infrared; GOX, Glucose oxidase; i.t., Intratumoral; MDR, Multidrug resistance; NaAlg, Sodium alginate; ROS, Reactive oxygen species; SDS-PAGE, Sodium dodecyl sulfate-polyacrylamide gel electrophoresis; TGD, Tumor growth delay; TPLD, Tumor plus leg diameter; XPS, X-ray photoelectron spectroscopy; α-MEM, Alpha-minimal essential medium; η, Intrinsic viscosity; η_{sp}, Specific viscosity.

GOX, which generates hydrogen peroxide in the presence of oxygen and glucose, has been shown to exhibit antitumor activity both *in vitro* and *in vivo* under physiological conditions (11–14) and efficacy in overcoming MDR in breast cancer cells (13,14). Because GOX is susceptible to degradation and denaturation, daily intratumoral injection of GOX was applied to inhibit tumor growth *in vivo* (11). To increase its stability, GOX was conjugated with polyethylene glycol and injected intravenously. However, repeated administration was still required to achieve a therapeutic effect (12). The low efficacy of systemically delivered GOX could be due to insufficient local ROS concentration in the tumor over time and the systemic toxicity of ROS to normal tissue. It is well-documented that blood vessels in solid tumors are abnormal and heterogeneous, which, together with the interstitial hypertension generated by proliferating cancer cells, impairs blood flow and thus drug delivery to tumor tissue (15–17). Although the leakiness of tumor vasculature has been utilized to deliver anticancer agents *via* macromolecule or nanoparticle carriers (18), this approach cannot deliver drugs to a large portion of tumor tissue where blood vessels are absent (17,19). To solve this problem, locoregional drug delivery to solid tumors has been investigated in preclinical and clinical settings (20–26).

Local delivery of therapeutic agents by microspheres and nanoparticles has been shown to enhance therapeutic efficacy because of increased local concentration of drug in tumors, extended exposure of tumors to toxic drug levels, and decreased systemic toxicity by reducing the drug concentration in the blood circulation (20–26). This treatment approach could be used **(1)** before surgery to shrink a tumour to a smaller size (also called neoadjuvant therapy), allowing conservative surgery, such as a lumpectomy, rather than a mastectomy, or **(2)** after surgery to reduce the chance of metastasis or recurrence (also called adjuvant therapy) by eliminating remaining cancer cells. Our laboratory has successfully developed biodegradable microspheres and polymer-lipid hybrid nanoparticles (13,14,22–28) for local delivery of doxorubicin, mitomycin C, paclitaxel and MDR reversing agents. Significant delays in tumor growth and even elimination of tumor recurrence and lymphatic metastasis have been achieved with these particulate formulations (22–26). We have also developed a microsphere formulation of GOX using an emulsification-internal gelation and polyeletrolyte coating method for production of ROS locally (13,14,28). GOX encapsulated in alginate/chitosan microspheres (ACMS-GOX) has been shown to effectively circumvent MRD *in vitro* (14). The enzymatic activity of GOX was maintained as demonstrated by prolonged production of H_2O_2 in glucose solutions (28). This sustained activity was superior to that of free GOX (FR-GOX) in terms of its potential to produce ROS *in situ* for locoregional treatment of solid tumors. To develop ACMS-GOX into a useful microsphere formulation for local oxidation therapy of tumor, a thorough understanding of the mechanism of GOX immobilization in the microspheres and evaluation of its *in vivo* efficacy are essential. Therefore, the present work was focused on these two aspects.

In the preparation of ACMS, ionic complexation was employed to form a crosslinked hydrogel due to the relatively inert aqueous environment within the matrix, the mild encapsulation condition at room temperature and the adjustable gel porosity allowing various diffusion rates of small and large molecules. The ACMS, however, may cause some steric hindrance and rigidification of the enzyme depending on whether the enzyme is present at the surface or encapsulated well inside the ACMS. As the binding of a substrate with the enzyme and the following reaction may be affected by the position of the enzyme in the microsphere, characterization of the enzyme distribution within the ACMS is necessary. In addition, the stability of proteins, possible interactions between the proteins, and the polymer matrix need to be better understood (29). Recent characterization of protein stability and enzymatic activity in relation to encapsulation methods and formulation processes was conducted with varying results (30–35). For instance, enhanced biological activity of vascular endothelial growth factor (VEGF) (30,31) and effectiveness of insulin in diabetic rats (32) were shown when they were released from alginate matrixes, whereas only up to 10% enzymatic activity remained in other studies (34,35). The reduction or loss of protein/enzymatic activity was, for the most part, ascribed to the interaction between the polymers, such as alginate and proteins. However, no direct evidence was presented how and in which step of the fabrication process they were deactivated.

This work was undertaken to investigate the effects of interactions between GOX, calcium alginate (CaAlg) and chitosan, and of the fabrication process, on the stability and bioactivity of encapsulated GOX. The mechanism of GOX loading into ACMS-GOX and the internal structure and molecular interactions in the ACMS-GOX were studied by various techniques, including Fourier transform infrared spectroscopy (FT-IR) and differential scanning calorimetry (DSC). Confocal laser scanning microscopy (CLSM) and X-ray photoelectron spectroscopy (XPS) were used to examine the distribution of GOX molecules within the ACMS. The *in vivo* effects and general toxicity of ACMS-GOX in a mouse breast tumor model were evaluated in comparison with GOX solutions. These studies will help optimize the formulation and preparation of ACMS-GOX for locoregional treatment of solid tumors.

MATERIALS AND METHODS

Materials

Chitosan, with a molecular weight of 150 kDa, was purchased from Fluka (Buchs, SG, Switzerland). Calcium carbonate, acetic acid and light mineral oil were obtained from Fisher Scientific (Fair Lawn, NJ, USA). Alginate (sodium salt, medium molecular weight, viscosity of 2.0% solution at 25°C, 3,500 cPs), glucose oxidase (Type X-S, 180U/mg, from *Aspergillus niger*), peroxidase (Type II, from horseradish), potassium persulfate, Span 80 and Tween 80 were purchased from Sigma (St. Louis, MO, USA). Distilled and deionized (DDI) water was prepared by a Millipore (Billerica, MA, USA) water-purification system. Cell culture medium, alpha-Minimal Essential Medium (α-MEM) with antibiotics (streptomycin and penicillin, 0.1 g/L each), was obtained from the Ontario Cancer Institute (Toronto, ON, Canada). Fetal bovine serum (FBS) was purchased from Cansera International Inc. (Etobicoke, ON, Canada). All cell culture plastic-ware was purchased from Sarstedt (Montreal, Quebec, Canada). PeroXOquant™ quantitative peroxide

assay kit (aqueous-compatible formulation) was purchased from Pierce (Rockford, IL, USA).

Chitosan Preparation and Characterization

A modified free radical method was employed to obtain low molecular weight chitosan (36). Fifteen grams of chitosan was dissolved in 1 l of 2% (v/v) acetic acid solution and heated to 70°C under constant stirring while being purged with nitrogen. Then 1.08 g of potassium persulfate was added to the reaction mixture. The reaction was stopped after 1 h by adding 400 ml of a 5% (w/v) aqueous solution of NaOH. The degraded chitosan was filtered and rinsed extensively with water. The molecular weight of the degraded chitosan was determined by a viscometric method using a calibrated Ubbelohde viscometer tube at 25±0.1°C (37). In brief, a series of 0.2, 0.5, 1.0, 1.5 and 1.8% (w/v) solutions of the degraded chitosan in 0.2 M NaCl/0.1 M CH_3COOH buffer was prepared and filtered through 0.45 μ membranes to eliminate undissolved particles. The specific viscosity (η_{sp}) of the chitosan solutions at different concentrations was then measured. The intrinsic viscosity (η) was obtained by extrapolating the linear plot of η_{sp}/concentration *vs.* concentration to zero concentration. The viscosity average molecular weight (Mv) was then calculated using the Mark-Houwink equation:

$$\eta = k \cdot Mv^{\alpha}$$

where $k=1.81\times10^{-3}$, $\alpha=0.93$.

The degree of deacetylation of the degraded chitosan was determined by an acid-base titration method (38). Briefly, 0.05 g of the degraded chitosan was dissolved in a 50 ml excess of 1 M HCl, and then the pH was titrated using a 0.1 M NaOH aqueous solution. The resulting titration curve had two inflection points related to the excess HCl and to the protonated amino groups. The degree of deacetylation (DD%) was calculated from the volume of NaOH consumed between the two inflection points by the following equation:

$$DD\% = \frac{16.1(y-x)f}{w} \times 100\%$$

where f is the molarity of NaOH, x and y stand for the amount of NaOH consumed at the first and second inflection point respectively, and w the weight of the degraded chitosan.

Formulation Preparation of GOX in ACMS

A modified emulsification-internal gelation method was employed to prepare CaAlg as described previously (28). In brief, 6.0 ml of 1.5% (w/v) sodium alginate solution containing 0.02 g of calcium carbonate was sonicated and then dispersed into 30 ml of light mineral oil containing 1.5% (v/v) Span 80 and 0.2% (v/v) acetic acid while stirring at a speed of 760 rpm at room temperature. Next, 120 ml of DDI water was added to the above emulsion and stirred for 40 min at a speed of 300 rpm. The CaAlg was rinsed with 200 ml of 1.0% (v/v) Tween 80 in aqueous solution and then by 100 ml of DDI water three times to remove any traces of light mineral oil. In a typical GOX loading experiment, 0.5 ml of CaAlg was added into 0.5 ml of 0.2 mg/ml (36 U/ml, i.e. 180 U/mg of solid GOX) GOX in a pH 4 buffer solution. The adsorption experiments were carried out for 30 min at 4°C. The GOX loaded CaAlg (CaAlg-GOX) gel beads were then coated with chitosan by incubation in 1% (w/v) chitosan solution for 10 min. During the coating process, the CaAlg was gently shaken at 4°C to make the reaction uniform.

GOX Distribution within ACMS

An EZ-label™ fluorescein isothiocyanate (FITC) protein labeling kit (Pierce, Rockford, IL, USA) was used to label GOX by following the protocol provided by the supplier. Briefly, the GOX solution was incubated with FITC for 1 h for the labeling reaction to take place. The reaction mixture was then applied to a desalting column to remove the unreacted FITC. The labeled GOX was loaded into ACMS using the same method used for the unlabeled GOX. The distribution of the labeled GOX was observed by CLSM (LSM510, Carl Zeiss, Jena, Germany). An argon laser provided an excitation wavelength of 488 nm. The emitted fluorescein light was detected at 510 nm, indicating the distribution of the labeled GOX in ACMS for various GOX loading and chitosan coating concentrations.

The distribution of unlabeled GOX within ACMS was also measured by XPS. The XPS spectra of samples of ACMS-GOX, blank ACMS, GOX, chitosan film, CaAlg, sodium alginate (NaAlg) film were obtained using a Leybold (Specs) MAX 200 XPS system (Specs GmbH, Berlin, Germany). The chitosan films and NaAlg films were obtained by casting the solution of chitosan and NaAlg onto a glass surface and were dried at room temperature. A non-monochromatised Mg Kα anode operated at 300 W (15 kV and 20 mA) was used for X-ray generation. The energy range measured, 280–540 ev, was calibrated against Cu $2p_{3/2}$ and Cu 3p lines at 932.7 and 75.1 eV, respectively. No differential charging was observed with the use of the non-monochromatic source. The energy scale was corrected by placing the C1s value for the main C–C component at 285 eV. Atomic ratios were obtained from spectra collected in a low-resolution mode, whereas other chemical information was obtained in the high-resolution mode. Spectral fitting was performed using the SpecsLab program (Specs GmbH, Berlin, Germany).

Sodium Dodecyl Sulfate Polyacrylamide Gel (SDS-PAGE) Analysis and GOX Release Test

To monitor the integrity of GOX in the formulation process, samples collected at each stage were analyzed by SDS-PAGE as described by Laemmli (39). In brief, 3 μg of GOX were denatured at 37°C for 15 min in Laemmli sample buffer containing 1% SDS and 100 mM dithiothreitol and electrophoresed through a 10% (*w/v*) polyacrylamide gel. The resulting gel was then stained and visualized by Coomassie Brilliant Blue R-25. Samples from each stage, i.e. freshly prepared GOX stock solution, GOX remaining in the adsorption medium after 30 min and GOX left in the medium after chitosan coating, were examined. A 10–250 kDa molecular weight marker (Amersham Biosciences, Buckinghamshire, UK) was used as molecular weight ladder. The concentration of GOX in buffer solutions was measured by the BioRad (Hercules, CA, USA) protein microassay. Here, 800μl of GOX sample was combined with 200 μl of Bio-Rad

assay dye and incubated at room temperature. After 10 min incubation, absorption at 595 nm was measured and protein concentration determined as per Bio-Rad protein microassay instructions. The GOX release test was carried out using 0.5 ml of ACMS-GOX (3.5 mg dry weight) in 10 ml of 0.2 M pH 6.0 and pH 7.4 (KH_2PO_4-NaOH) buffer solutions at 37°C.

FT-IR Analysis

The FT-IR transmission spectra (Spectrum One spectrometer, PerkinElmer, Wellesley, MA, USA) were collected using potassium bromide disks. The samples of CaAlg gel beads, GOX, CaAlg gel beads after adsorption of GOX (CaAlg-GOX) and ACMS-GOX were freeze-dried, and a total of 2% (w/w) of samples were mixed with potassium bromide. The mixtures were ground into fine powders, and disks were compressed for scanning. Each sample was done at least in triplicate.

DSC Analysis

Thermograms of GOX, CaAlg gel beads, CaAlg-GOX, chitosan, blank ACMS and ACMS-GOX were obtained using a DSC-2010 system (TA Instruments, New Castle, DE, USA). Lyophilized samples (5–7 mg) were heated in crimped standard aluminum hermetic pans from 25 to 300°C at a heating rate of 10°C per min with a constant purging of nitrogen at 50 ml per min. The system was calibrated with indium (melting point of 156.86°C). The characteristic peaks of the melting endotherm of all the samples were recorded (40). Each sample was measured at least in triplicate.

Determination of the Activity of GOX

The activity of GOX was evaluated by measuring the kinetics of H_2O_2 generation. H_2O_2 concentrations in the culture medium were determined using a PeroXOquant™ quantitative peroxide assay kit. At different time intervals, 800 µl of the culture medium was taken and centrifuged for 1 min through a Centricon® YM-50 (Millipore, Billerica, MA, USA) which has a cut-off molecular weight of 50 kDa. Then, 20 µl of filtrate was added to a 200 µl of assay kit solution and incubated for 15 min at room temperature and assayed using a microplate reader (Molecular Device, Sunnyvale, CA, USA) at 595 nm.

In Vitro Cytotoxicity of ACMS-GOX

All *in vitro* cytotoxicity experiments were carried out using EMT6 murine breast cancer cells generously provided by Dr. R. P. Hill (Ontario Cancer Institute, Toronto, Canada). Cells (5th–30th passages in our hands) were grown as a monolayer in 75 cm^2 cell culture flasks containing 25 ml of α-MEM with antibiotics (streptomycin and penicillin, 0.1 g/l each) supplemented with 10% FBS (defined as growth medium), in a humidified incubator with 5% CO_2/95% air at 37°C. Confluent cultures were trypsinized with 0.05% trypsin-EDTA (ethylene-diamine-tetra-acetic acid) (Invitrogen, Burlington, ON, Canada) and subcultured twice a week.

Twenty-four hours prior to treatment, 5×10^5 cells were seeded in 10 cm Petri dishes containing 10 ml of growth medium. Aliquots of FR-GOX or ACMS-GOX were incubated with cells for 1 h. ACMS-GOX were prepared by incubating CaAlg (3.95 mg) in 0.5 ml of 0.4 U/ml, 2 U/ml, 6 U/ml and 10 U/ml GOX with an encapsulation efficiency of 80%, respectively. Following incubation of cells, the cells were rinsed with PBS and then trypsinized. The resuspended cells were counted with a hemocytometer and plated at various dilutions (100, 1,000, 10,000 cells/dish) in duplicate in 6 cm Petri dishes containing 5 ml of growth medium. After 6 to 7 days, the macroscopic colonies formed by viable cells were fixed and stained with a 0.5% solution of methylene blue in 50% ethanol. Plating efficiencies were determined by the number of colonies formed divided by the number of cells plated in the Petri dishes. Normalized surviving fractions of cells were then obtained by dividing the plating efficiency of the drug-treated cells by that of cells without treatment (41). The experiments were repeated in triplicate. The control plating efficiency of EMT6 cells was 0.49±0.07 (n=10).

In Vivo Evaluation of Efficacy and General Toxicity of Treatments

Nine to ten week-old female BALB/c mice (Taconic, Germantown, NY, USA) were inoculated intramuscularly in the hind leg with 5×10^5 EMT6 cells in 50 µl of the growth medium at least one week after the mice were received. The treatments were initiated when the tumor-plus-leg diameter (TPLD) reached approximately 8–9 mm (about 0.3 g of tumor), an average of 4–6 days following inoculation. On the day of treatment (day 0), the mice were randomized into groups of 4–5 animals each. The dose for ACMS-GOX was 1,000 U/kg, approximately equal to 20 U/mouse, and was delivered by 0.105 mg of GOX loaded in 0.13 mg of microspheres. FR-GOX injected i.t., blank (unloaded) microspheres (0.13 mg of microspheres injected i.t.) and control (no treatment) groups were included for comparison. All animal studies were performed under a protocol approved by the Animal Care Committee at the Ontario Cancer Institute (Toronto, ON, Canada).

The TPLDs were measured daily for the first 7 days and then at least every other day by passing the tumor-bearing leg through a plastic plate containing a series of circular holes whose diameters increased in 0.5-mm steps. When the TPLD reached 12.5 mm, corresponding to an average tumor weight of 1.0 g, the animals were sacrificed, and the time was recorded. Once the animals were sacrificed, tumors were excised, weighed and stored in formalin for future examination. The various treatment groups are listed in Table III. The efficacy of the treatment was evaluated by determining the tumor growth delay (TGD). Tumor growth delay was calculated using the following equation:

$$TGD = (T_{treat} - T_{control})/T_{control} \times 100\%$$

where T_{treat} and $T_{control}$ represent the average number of days for tumors to grow to the end point of 12.5 mm TPLD for the treatment group and control group, respectively (23).

Systemic toxicity of the treatments was characterized semi-quantitatively by measuring the weight-loss of the mice

daily as described previously with modifications (22–24). A general toxicity score of 0, 1 or 2 was assigned to each animal as an indication of body weight-loss (0 = no weight-loss, 1 = 1–2 g weight-loss, 2 = 2 g or more weight-loss). Greater than 20% weight-loss in initial animal body weight was considered to be a severe systemic toxicity, and the mouse was sacrificed for a humane end-point. In addition, general toxicity was monitored by degree of fur-roughing, general activity and tissue damage at the site of injection of the mice.

Tumor Morphological and Histological Evaluation

Tumor tissues were randomly collected from each treatment group for histological analysis as a part of the toxicity study. Tumors were excised and sectioned into halves and photographed for morphological study. The tissue slides used Hematoxylin & Eosin (H & E) staining.

Statistical Analysis

Experiments to determine the *in vitro* activity of ACMS-GOX and FR-GOX were repeated at least three times. The results are expressed as means ± S.D. Statistical analysis for unpaired experimental data was performed using Student's *t* test between two groups. Two-way ANOVA analysis was performed to compare the differences for more than two groups. In all analysis, a value of $p<0.05$ was considered a significant difference.

RESULTS

Chitosan Preparation and Characterization

Low molecular weight chitosan was obtained using the free radical method (see materials and methods). A linear curve was acquired by plotting the η_{sp}/concentration *vs*. concentration of 0.2, 0.5, 1.0, 1.5 and 1.8% (*w*/*v*) degraded chitosan solutions. The intrinsic viscosity of 0.497 ml/g was obtained by extrapolating the linear plot of η_{sp}/concentration *vs*. concentration to the zero concentration. The molecular weight of the degraded chitosan was calculated as 59.3 kDa based on the Mark-Houwink equation. A 80.5% degree of deacetylation was determined by acid-base titration (data not shown).

GOX Distribution within ACMS

As seen in the CLSM images taken on a plane half-way through the microspheres (Figs. 1a–c), the FITC-labeled GOX distribution was not homogeneous within ACMS. Greater fluorescence intensity was observed near the surface (around 20 μm from the outer surface) than inside the ACMS as illustrated by the images and the fluorescence intensity curves, indicating that more FITC-labeled GOX molecules were located near the surface of ACMS. Around 40 units of fluorescence intensity were detected inside ACMS, whereas around 60 units were present near the surface with a 0.5 mg/ml GOX loading solution and 1% chitosan coating (Fig. 1a). With 0.5% chitosan coating and the same GOX loading concentration (Fig. 1b), 2-fold greater, around 80 units of fluorescence intensity, were found inside ACMS and approximately 120 units near the surface. When the GOX loading concentration was increased to 1.5 mg/ml with a 1% chitosan coating, a 3-fold increase, around 120 units of fluorescence intensity were detected inside ACMS and around 240 units near the surface (Fig. 1c). Fig. 1d shows the distribution of GOX within ACMS by displaying 20 optical sections of 4.3 μm in a "z-stack" scan of a FITC-labeled GOX-loaded microsphere from the top to the bottom. The microsphere was compressed (about half-flattened) due to the weight of the cover slide resulting in a larger "diameter" and a smaller number of optical sections than would be expected for a sphere.

The GOX distribution within ACMS was investigated further using XPS. This method can quantitatively evaluate the elemental composition of the outermost portion, 2 to 10 nm of the samples (42). Table I compares the elemental composition of the surfaces of ACMS-GOX, blank ACMS, GOX, CaAlg gel beads, chitosan films and NaAlg films. The elemental composition was calculated from the XPS spectra recorded in low-resolution mode and is expressed as relative atomic percentage. The surface of ACMS-GOX was composed primarily of 65.5% C, 27.9% O, 3.8% N and 0.4% Ca. These elements are the primary components of blank ACMS (69% C, 26.6% O, 2.1% N and 0.2% Ca) and GOX (65.8% C, 27.1% O and 6.3% N), indicating that each substance was present within the outer 10 nm of ACMS. For example, ACMS-GOX has 0.4% Ca and GOX has no Ca, which means the element Ca was from CaAlg (1.7% Ca) or blank ACMS (0.2% Ca). Therefore, CaAlg was present on the surface. Similarly, ACMS-GOX has 3.8% N, whereas blank ACMS and GOX have 2.1% N and 6.3% N, respectively. Additionally 2.4% silicon was detected in ACMS-GOX, which was probably from an impurity of calcium carbonate (blank ACMS, 2.0% Si).

In order to confirm the origin of the elements detected by XPS, the C1s, O1s, and N1s peaks of the XPS spectra were deconvoluted at high resolution as seen in Fig. 2. The chemical groups associated with each deconvoluted peak were identified by their characteristic binding energies. The C1s (Fig. 2a), O1s (Fig. 2b) and N1s (Fig. 2c) peaks of ACMS-GOX appear to be made up of the overlapping of C1s, O1s and N1s peaks of blank ACMS and GOX. For example, for the blank ACMS, the N1s peak (Fig. 2c) with binding energy of 399.3 eV was from the acetamide groups (–HN–C = O) of chitosan molecules. For GOX, the characteristic N1s peak with binding energy of 400 eV was attributed to the amide groups (–HN–C = O) in GOX molecules. The N1s peak with binding energy around 400 eV of ACMS-GOX is an overlap of the –HN–C = O groups from both blank ACMS and GOX. These results were consistent with unlabeled GOX molecules being present in the outer layer of the ACMS. In Table I, the ratio of carbon to nitrogen for ACMS-GOX (17.2) was much smaller than that of blank ACMS (32.9) and higher than that of GOX (10.4), also indicating the presence of GOX near the surface of ACMS.

Integrity of GOX in ACMS Formulation

SDS-PAGE is a standard method used to investigate the integrity of proteins via determination of change in its molecular weight on the gel. Fig. 3 compares GOX released for 2 h (Lane 1), 8 h (Lane 2), 24 h (Lane 3) and the molecular weight marker (Lane 4). There is no change in the

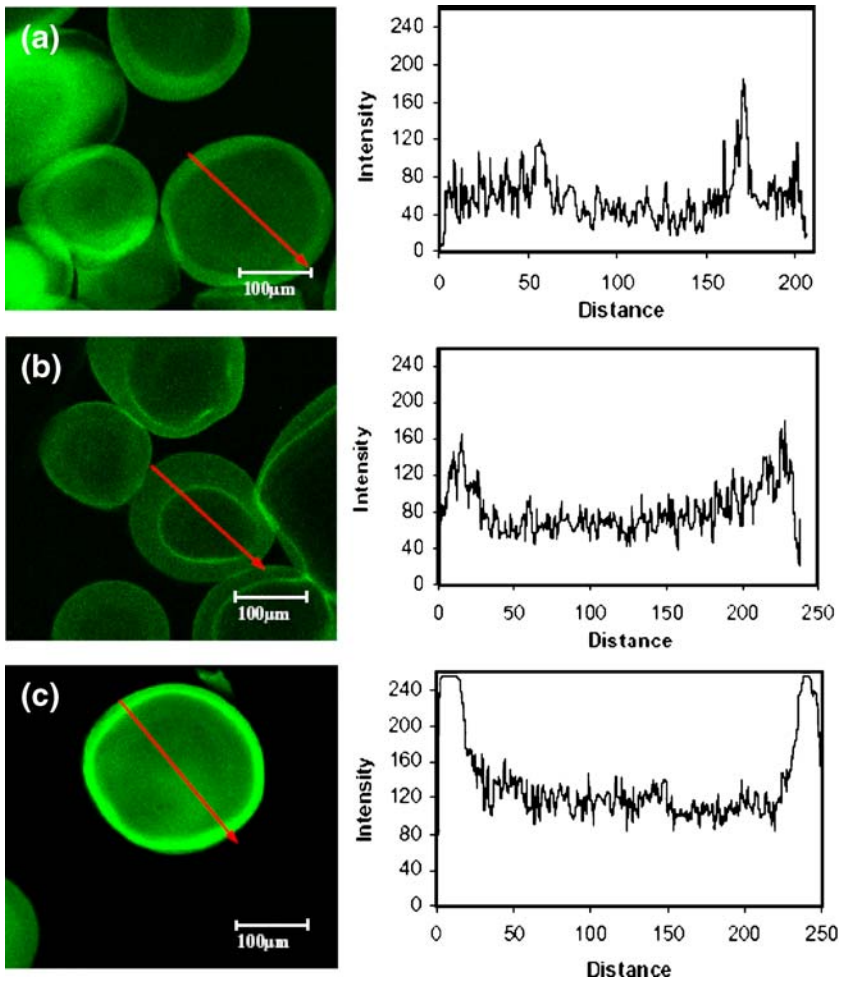

Fig. 1. Confocal laser scanning microscopy (CLSM) images of the distribution of fluorescein isothiocyanate (FITC)-labeled glucose oxidase (GOX) within alginate/chitosan microspheres (ACMS) and fluorescence intensity along the diameter arrow with (**a**) 0.5 mg/ml GOX loading solution, 1% chitosan coating, (**b**) 0.5 mg/ml GOX loading solution, 0.5% chitosan coating, (**c**) 1.5 mg/ml of GOX loading solution, 1% chitosan coating, and (**d**) "z-stack" scanning of the microsphere with 4.3 μm optical section for each slice for microspheres prepared with 1.5 mg/ml of GOX loading solution and 1% chitosan coating.

migration of the three GOX bands on the gel and the protein existed as 80-kDa monomeric subunit, indicating that the GOX after release neither aggregated nor degraded. GOX present in the absorption medium and after coating with chitosan also remained as an 80-kDa band (data not shown). Because the reduced SDS-PAGE technique was used, the disulfide bond linked dimer of native GOX was likely broken and thus the dimer is not seen in either freshly prepared GOX sample or samples after loading and coating.

FT-IR Spectrum of GOX and ACMS-GOX

The transmission FT-IR spectra of CaAlg gel beads, GOX, CaAlg-GOX and ACMS-GOX are depicted in Fig. 4. The bands observed at 1,610 cm^{-1} and 1,424 cm^{-1} in the spectrum of CaAlg gel beads (Fig. 4a) correspond to asymmetric and symmetric stretching peaks of carboxylate salt groups, respectively (43). The peaks at 1,300 cm^{-1} (C–O stretching), 1,090 cm^{-1} (C–O stretching), 1,035 cm^{-1} (C–O–C stretching), and 1,135 cm^{-1} (C–C stretching) are attributed to its saccharide structure. The GOX spectrum (Fig. 4b) shows the characteristic peaks of protein amide at 1,650 cm^{-1} (Amide I, C = O stretching) and 1,597 cm^{-1} (Amide II, N–H bending, C–N and C–C stretching). The new bands at 2,500 cm^{-1} and 1,950 cm^{-1} verify the presence of $-NH_3^+$ group in the CaAlg-GOX spectrum (Fig. 4c). The new band appearing at 1,560 cm^{-1} could be assigned to symmetric $-NH_3^+$ deformation. The peak at 1,265 cm^{-1} can be ascribed to $-COO^-$ symmetric stretching of CaAlg-GOX. These results indicate that an electrostatic interaction occurred between CaAlg and GOX. However, the amide I peak of GOX (1,650 cm^{-1} was still present in the spectrum of CaAlg-GOX (Fig. 4 c) and ACMS-GOX (Fig. 4d) but shifted to 1,655 cm^{-1} for ACMS-GOX. These results indicate that the essential features of native GOX did not change after being absorbed into CaAlg gel beads and coated with chitosan.

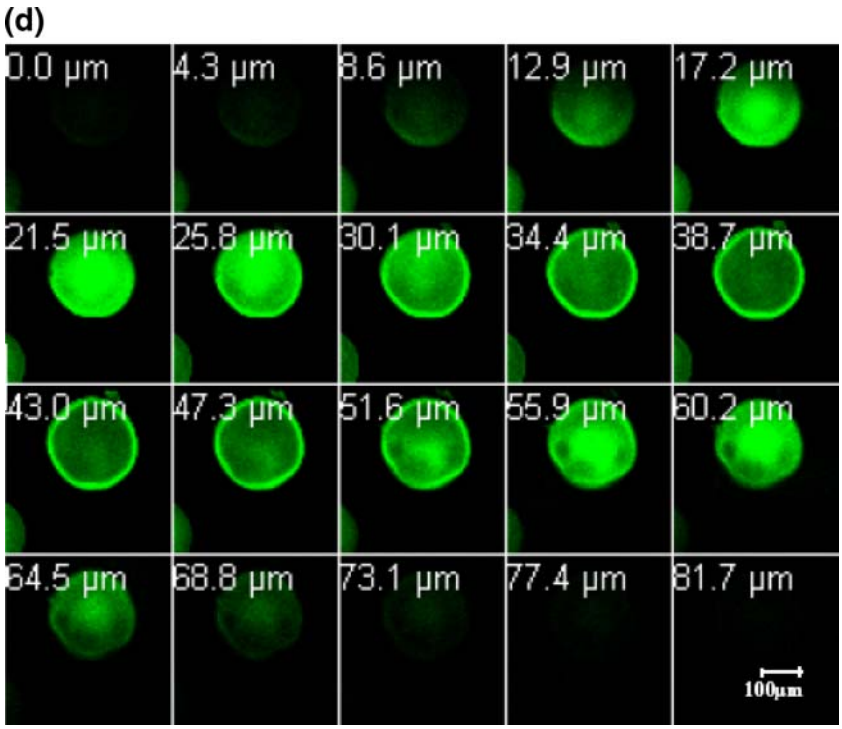

Fig. 1. (continued).

DSC Spectra of GOX and ACMS-GOX

DSC themograms of GOX, CaAlg gel beads, CaAlg-GOX, chitosan, ACMS and ACMS-GOX are represented in Fig. 5. GOX shows three characteristic endothermic peaks (Fig. 5a), which are identified as the glass transition temperature (T_g) at 50°C, the denaturation endotherm at 124°C and the melting point at 168°C according to Kennamer (44) and Sarti (45). The exothermic peak at 279°C is associated with the decomposition of the GOX. The DSC thermogram of CaAlg gel beads (Fig. 5b) exhibits one endothermic peak and one exothermic peak at 158°C and 251°C, corresponding to the melting and decomposition temperatures, respectively. After the adsorption of GOX into CaAlg gel beads (Fig. 5c), the glass transition peak and denaturation peak of GOX at 50°C and 124°C disappeared. The melting peak of GOX

Table I. Surface elemental composition of glucose oxidase encapsulated in alginate/chitosan hydrogel microspheres (ACMS-GOX), blank alginate/chitosan hydrogel microspheres (ACMS), glucose oxidase (GOX), calcium alginate (CaAlg) gel beads, chitosan films and sodium alginate (NaAlg) films calculated from X-ray photoelectron spectroscopy (XPS) spectra recorded in low-resolution mode and expressed as relative atomic percentages and ratio of two elements

	ACMS-GOX	Blank ACMS	GOX	CaAlg gel beads	Chitosan film	NaAlg film
C[a]	65.5	69.0	65.8	62.6	61.1	56.8
O	27.9	26.6	27.1	33.5	31.5	33.3
N	3.8	2.1	6.3	0.1	5.9	1.0
Ca	0.4	0.2	0.0	1.7	0.1	0.1
Na	0.0	0.0	0.0	0.4	0.9	6.9
Cl	0.0	0.0	0.0	0.1	0.1	0.6
P	0.1	0.1	0.1	0.1	0.1	0.1
S	0.0	0.0	0.2	0.1	0.2	0.9
Si	2.4	2.0	0.4	1.4	0.1	0.3
C/N[b]	17.2	32.9	10.4	62.6	10.4	56.8
C/Ca	163.8	345	N/A	36.8	611	568
C/O	2.35	2.59	2.43	1.87	1.94	1.71

[a] Values are presented as percentage
[b] Values are presented as ratio of two elements

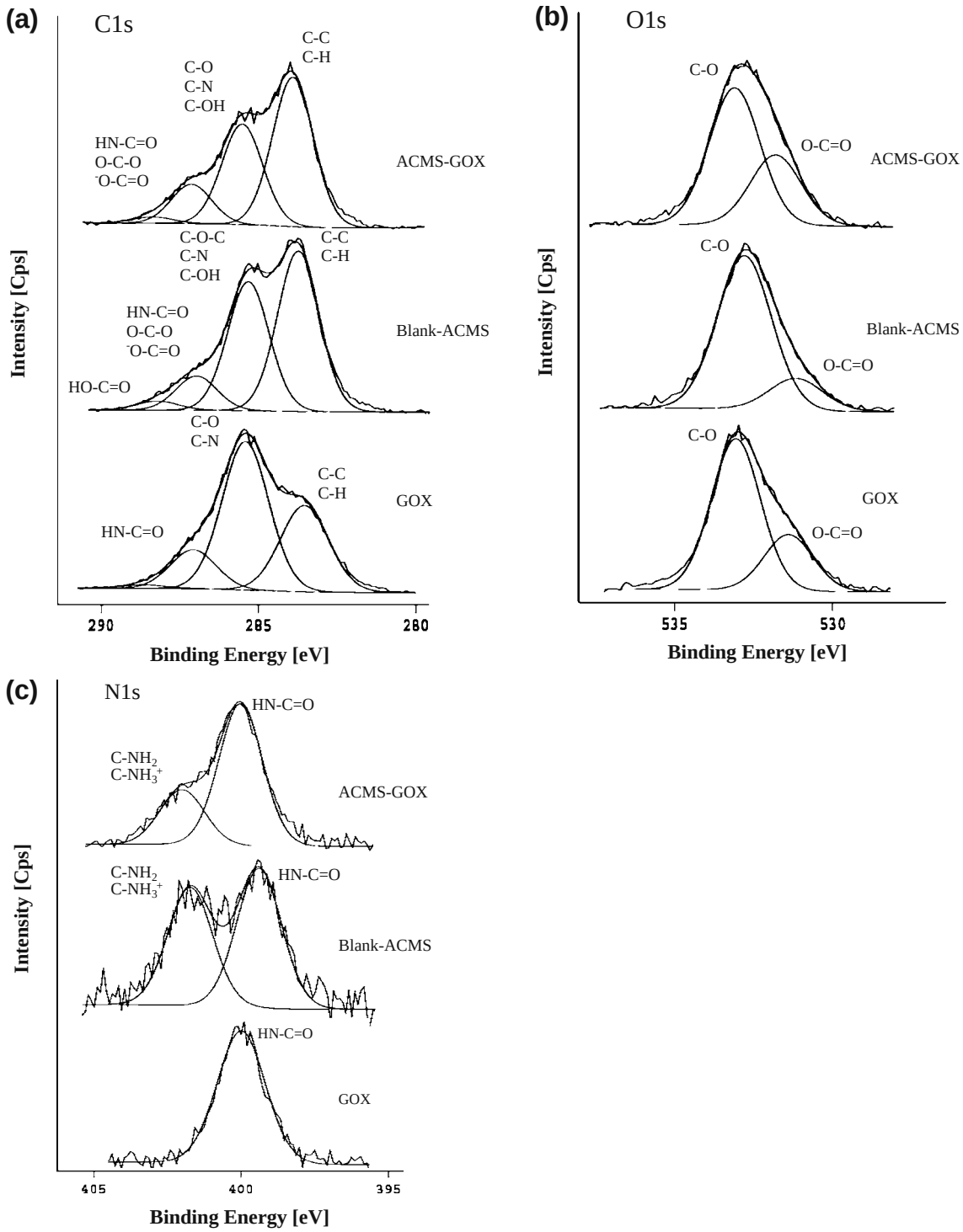

Fig. 2. X-ray photoelectron spectroscopy (XPS) spectra of (**a**) C1s, (**b**) O1s and (**c**) N1s for GOX encapsulated ACMS (ACMS-GOX), blank ACMS and GOX recorded and deconvoluted in high-resolution. ACMS-GOX was prepared with 1 mg/ml GOX loading solution and 1% chitosan coating.

coalesced with the melting peak of CaAlg gel beads and formed a wider endothermic peak at 187°C. Chitosan has a melting peak at 162°C (Fig. 5d). The blank ACMS has a melting endotherm at 173°C (Fig. 5e), which is higher than either CaAlg gel beads or chitosan itself. After loading of GOX, the melting endotherm of ACMS shifted to a higher temperature at 180°C and became wider (Fig. 5f).

Determination of the Activity of GOX

Table II compares the concentration of H_2O_2 generated at different times by FR-GOX and ACMS-GOX containing equivalent amounts of GOX. In Table II, FR-80 represents 80 mU/ml free GOX, ACMS-80 stands for 80 mU/ml ACMS-GOX equivalent to free GOX. The ACMS-GOX were

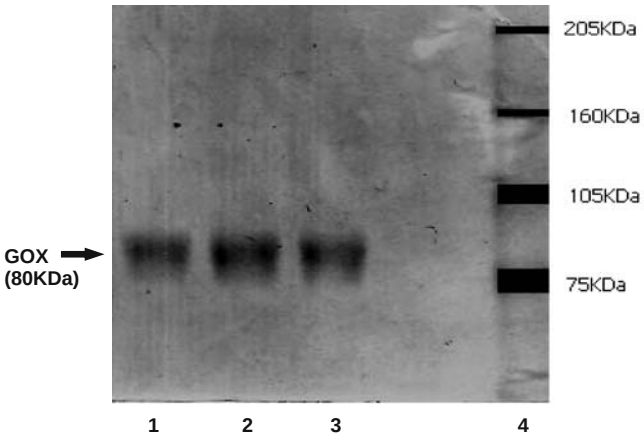

Fig. 3. Reduced sodium dodecyl sulfate polyacrylamide gel (SDS-PAGE) of GOX samples collected from release medium. Approximate 3 μg GOX samples were added to each lane. Lane 1–3, GOX after release for 2 h, 8 h and 24 h, respectively; Lane 4, molecular weight marker; Lane 1–3 exhibit bands of 80-kDa monomeric subunits of GOX.

prepared by incubating CaAlg gel beads in 0.5 ml of 2 U/ml (ACMS-80) and 10 U/ml (ACMS-400) respectively. The encapsulation efficiency of GOX was 80% in both cases. At the 5 h time interval, the concentration of H_2O_2 generated by ACMS-400 and FR-400 reached 1.68±0.17 and 1.30±0.05 mM, respectively, the former is 1.29-fold greater than the latter. This result indicates the activity of GOX was well retained in ACMS. However, at 1 h the concentration of H_2O_2 generated by ACMS-400 was less than that of FR-400, 0.38±0.07 and 0.59±0.02 mM, respectively. At the lower dose of GOX, the concentration of H_2O_2 generated by FR-80 and by ACMS-80 reached 0.44±0.02 and 0.31±0.06 mM in 5 h, respectively.

In Vitro Cytotoxicity of ACMS-GOX

The *in vitro* cytotoxicity of ACMS-GOX against EMT6 murine breast cancer cells is compared with that of FR-GOX at equivalent doses for different times of exposure in Fig. 6. Both ACMS-GOX and FR-GOX exhibit dose-dependent and

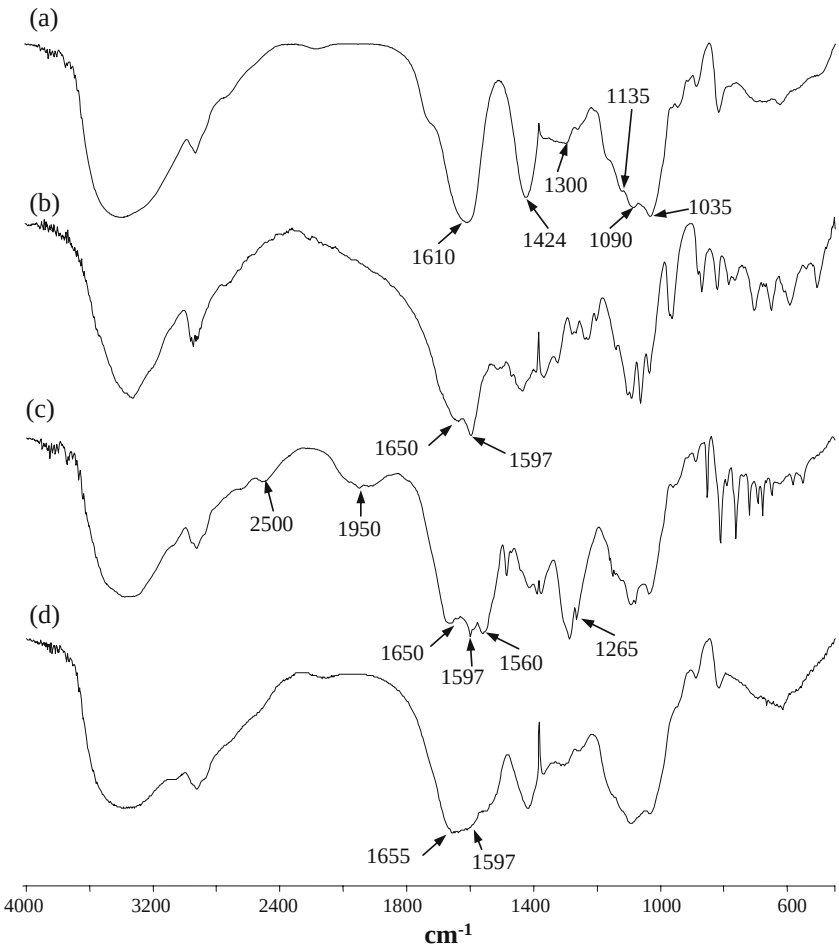

Fig. 4. Transmission Fourier transform infrared spectroscopy (FT-IR) spectra of (**a**) CaAlg, (**b**) GOX, (**c**) CaAlg-GOX and (**d**) ACMS-GOX obtained from 2% (*w*/*w*) of the samples compressed in around 100 mg of potassium bromide disks. ACMS-GOX was prepared using 1 mg/ml GOX pH 4 buffer solution as loading solution and 1% chitosan coating. Each experiment was repeated at least in triplicate.

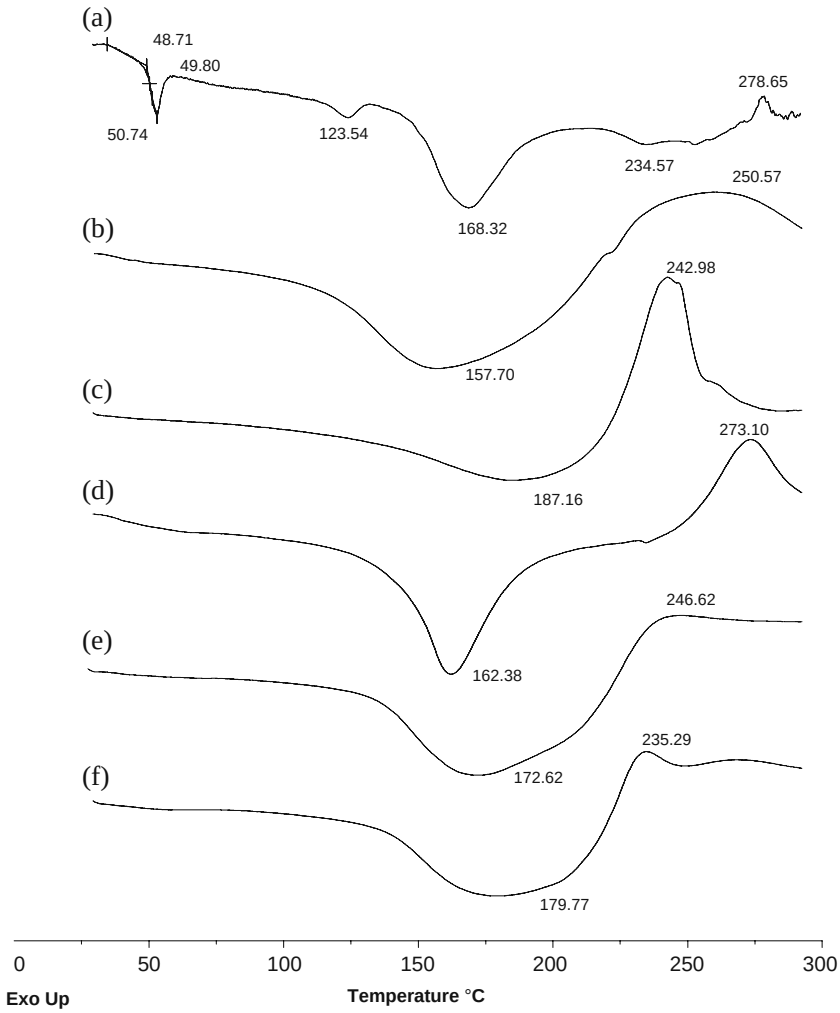

Fig. 5. Differential scanning calorimetry (DSC) themograms of (**a**) GOX, (**b**) Calcium alginate (CaAlg), (**c**) CaAlg-GOX, (**d**) chitosan, (**e**) blank ACMS, and (**f**) ACMS-GOX. All the samples were heated from 25° to 300°C at a heating rate of 10°C per min with a constant purging of nitrogen at 50 ml per min. ACMS-GOX were prepared using 1 mg/ml GOX pH 4 buffer solution as loading solution and 1% chitosan coating. Each experiment was repeated at least in triplicate.

time-dependent cytotoxicity. However, ACMS-GOX exibited less cytotoxicity than the FR-GOX for all times of exposure. The dose for 90% cell killing of ACMS-GOX was 3.4-fold greater than FR-GOX, around 360 mU/ml *versus* 105 mU/ml respectively, for 1 h exposures. At 3 and 5 h exposures, this differential in cell killing of FR-GOX *versus* ACMS-GOX was manitained or increased. The blank ACMS did not show cytotoxicity to EMT6 tumor cells (data not shown).

Table II. Concentration of H_2O_2 generated by free GOX (FR-GOX) and ACMS-GOX as a function of GOX concentration and time

	Hydrogen peroxide concentration (mM)[a]		
Concentration of GOX (mU/ml)	1 h	3 h	5 h
FR-80[b]	0.10±0.01	0.27±0.02	0.44±0.02
ACMS-80	0.04±0.01***	0.10±0.03***	0.31±0.06*
FR-400	0.59±0.02	1.12±0.04	1.30±0.05
ACMS-400	0.38±0.07**	1.23±0.10	1.68±0.17*

[a] Values are expressed as mean ± S.D. of three independent experiments
[b] FR-80 stands for 80 mU/ml free GOX, ACMS-80 stands for 80 mU/ml ACMS-GOX equivalent to free GOX. ACMS-GOX were prepared by incubating CaAlg gel beads (3.95 mg) in 0.5 ml of 2 U/ml (ACMS-80) or 10 U/ml (ACMS-400) GOX with an encapsulation efficiency of 80% in both cases
*$p<0.05$, **$p<0.01$, ***$p<0.001$, indicating significant difference between H_2O_2 generation by GOX in free form and encapsulated form

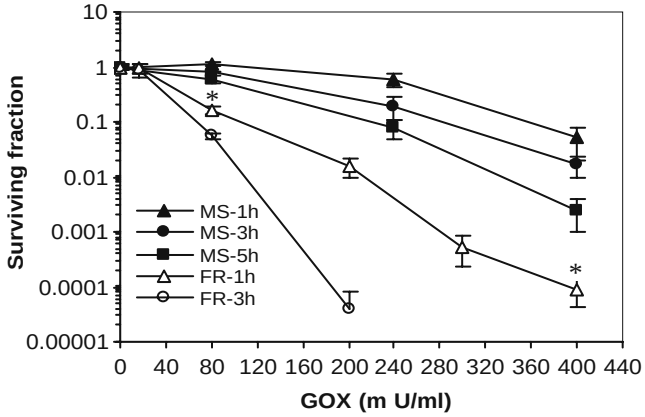

Fig. 6. *In vitro* cytotoxicity of free GOX (FR-GOX) and ACMS-GOX against EMT6/WT breast cancer cells after different time of exposure to either FR-GOX or ACMS-GOX at equivalent doses. The data points and the error bars represent mean ± S.D. (n=3); where not seen, the S.D. values lie within the symbols. * p<0.005, indicating significant difference between the treatment of ACMS-GOX-5h and FR-GOX-1 h.

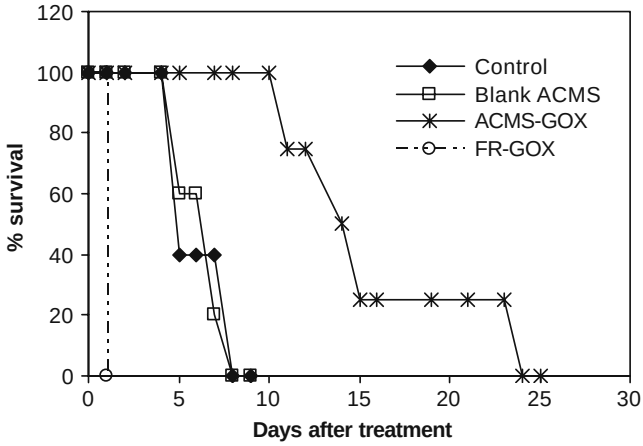

Fig. 7. "Percent survival" of groups of BALB/c mice bearing EMT6/WT tumor after intratumoral injection of ACMS-GOX or an equivalent dose of FR-GOX. The dose for ACMS-GOX is 1,000 U/kg, equal to 20 U/mouse, equal to 0.1052 mg of GOX loaded in 0.13 mg of microspheres. Comparison groups were injected with blank (unloaded) microspheres as a placebo (0.13 mg of microspheres) or control (no treatment). Each group contained four to five mice. "Percent survival" is the time for tumor to grow from 0.3 g to 1 g at which time the mice were sacrificed for humane reasons.

Efficacy of Intratumoral Delivery of ACMS-GOX

The efficacy of various intratumoral (i.t.) injection treatments in BALB/c mice bearing EMT6 tumor was evaluated by the tumor growth delay. Table III summarizes the efficacy of the various treatments. A tumor growth delay of 185% was observed in the group of mice receiving ACMS-GOX-1,000 U/kg. No tumor growth delay was obtained in the mice treated with the low dose of ACMS-GOX-500 U/kg. For the mice treated with i.t. administration of free GOX at both high and low doses (FR-GOX-1,000 U/kg and FR-GOX-500 U/kg), the mice became extremely lethargic on the second day indicating severe systemic toxicity. The mice were sacrificed shortly after their low general activity was seen. The group of mice receiving blank ACMS did not elicit any statistically significant tumor growth delay, indicating that blank ACMS has no antitumor effect in this model.

Fig. 7 represents preliminary results for tumor growth in BALB/c mice bearing EMT6 tumors and treated with ACMS-GOX. Percent survival is the time for tumor to grow from 0.3 g to 1 g. About a 2-fold increase in time for 50% of the tumors to grow to 1 g was observed when treated with 1,000 U/kg ACMS-GOX compared to blank ACMS and control. The FR-GOX group was sacrificed on the second day due to severe systemic toxicity. Hence no growth data can be reported afterwards.

General Toxicity of Intratumoral Delivery of ACMS-GOX

In contrast to the FR-GOX treated group, little systemic toxicity was observed in the group treated by the ACMS-GOX formulation compared to the control and blank ACMS treatment groups. In general, no tissue damage was found at the injection sites of the mice and no weight loss of over 20% was seen in any of the four groups. No significant animal weight loss was observed after i.t. injection of the ACMS-GOX treatment group compared to the control group (data now shown). For FR-GOX treatment groups at both doses, the mice were inactive, trembling and fur-roughing, and thus were sacrificed due to humane considerations. As also shown

Table III. Summary of treatment groups, tumor growth times, tumor growth delay and average toxicity score of each group: (1) control, (2) blank ACMS, (3) ACMS-GOX-1,000 U/kg, (4) FR-GOX-1,000 U/kg and (5) FR-GOX-500 U/kg

Trial#	Groups[a]	Time (days) to reach TPLD=12.5 mm (Mean ± S.D.)	TGD[b]	Average of Toxicity Scores (Ave ± S.D.)
1	Control	5.2±1.6	–	0.48±0.95
2	Blank ACMS	5.4±1.3	3.9%	0.42±0.58
3	ACMS-GOX-1,000	14.8±5.7*	184.6%	0.50±0.81
4	FR-GOX-1,000	n.a.[c]	n.a.	n.a.
5	FR-GOX-500	n.a.	n.a.	n.a.

[a] Each treatment group contained 4–5 mice

[b] Tumor growth delay (TGD) = $(T_{treat} - T_{control})/T_{control} \times 100\%$, where T_{treat} and $T_{control}$ represent the mean number of days for TPLD to reach 12.5 mm (corresponding to 1 g tumors) following treatment initiation for the treatment and control groups

[c] Data not available because the mice were sacrificed on the second day due to obvious systemic toxicity

*p<0.005, indicating significant difference among control, blank ACMS and ACMS-GOX-1,000 treatment groups by ANOVA analysis

in Table III, the average general toxicity scores for mice with i.t. injection of blank ACMS and both doses of ACMS-GOX are similar to the control group. This result suggests that i.t. delivery of ACMS-GOX causes minimal systemic toxicity and the blank ACMS is a safe carrier. The toxicity score in the group of mice receiving ACMS-GOX-500 exhibited higher values compared to the other groups.

Histological Evaluation of Tumor Tissue after Treatment

The internal structure of tumors randomly excised from an untreated control group animal and high dose ACMS-GOX treated mouse are shown in Fig. 8a, b. The tumor interior of untreated control group (Fig. 8a) seems solid and uniform throughout the whole tumor tissue. However, in the tumor excised from the mouse receiving i.t. delivery of ACMS-GOX-1,000 U/Kg (Fig. 8b), the tumor interior appears irregular with necrotic cavities. This indicates that locally delivered GOX may exert a tumorcidal effect within the tumor mass.

A representative microscopic view of H & E stained tumor tissue from the control group and the group receiving ACMS-GOX-1,000 U/kg are shown in Fig. 8c, d. A large area of necrosis is seen in the ACMS-GOX treated tumor tissue (Fig. 8d) which is greater than that in control tumor tissue. This result is consistent with the gross examination of the tumor interior.

DISCUSSION

Distribution of GOX within ACMS and GOX Loading Mechanism

The presence of FITC labeled GOX in the core of ACMS confirmed our hypothesis that the high porosity of CaAlg gel beads fabricated by the internal gelation method facilitated the diffusion of GOX into CaAlg gel beads leading to high GOX loading. The concentration gradient near the surface of ACMS may be explained by the complex formed

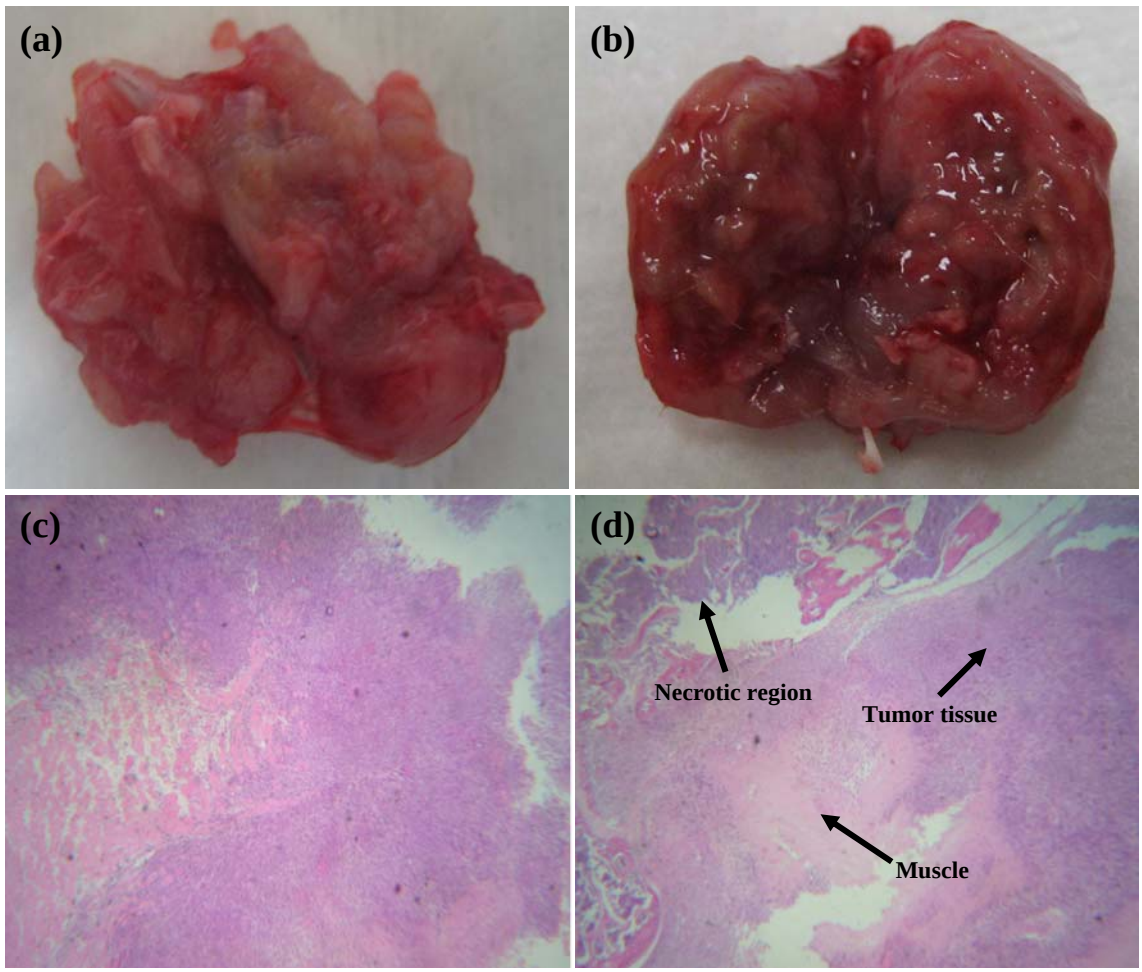

Fig. 8. The morphology of EMT6/WT tumors cross-sectioned along the longitudinal midline to expose their internal structure after treated with (**a**) blank ACMS or (**b**) ACMS-GOX-1,000 U/kg; and microscopic histological examination of a representative sections of tumor tissue after H&E staining for individual tumors taken from mice treated with (**c**) blank ACMS or (**d**) ACMS-GOX-1,000 U/kg. The blank ACMS as a control (0.13 mg of microspheres) (**a**, **c**) and ACMS-GOX-1,000 U/kg (equal to 20 U/mouse, 0.1052 mg of GOX loaded in 0.13 mg of microspheres) (**b**, **d**) were administered intratumorally to 0.3 g of EMT6/WT tumors growing in the hind legs of BALB/c mice. Tumors that grew to 12.5 mm of TPLD (1 g of tumor) were excised and preserved in 10% buffered formalin.

between CaAlg and GOX. The formation of a CaAlg and GOX complex could reduce the gel porosity and hinder the further diffusion of GOX into CaAlg gel beads. In addition, the greater GOX fluorescence intensity with a lower concentration chitosan coating revealed that a competition occurs between GOX and chitosan for the carboxylic group binding sites of CaAlg gel beads (28). Therefore, GOX was loaded mainly by its electrostatic interaction oppositely charged CaAlg.

Stability and Activity of ACMS-GOX and Interaction of GOX with Polymer Matrix

The H_2O_2 generation behavior and the absence of extra bands in the SDS-PAGE revealed that GOX was unchanged in intermit and final products. Two factors may contribute to the stability of GOX in the CaAlg and ACMS. Firstly the hydrophilic solid interface of CaAlg gel beads induces less structural changes when compared to a more hydrophobic interface between organic solvent and water (46). Secondly the electrostatic interaction between CaAlg and GOX could increase the stability of GOX. Although the mechanism of enzyme stability in aqueous solution is different from that in solid state (44,45), the strong interaction of CaAlg with GOX is evident in thermal analysis. After adsorption of GOX into CaAlg gel beads, the melting peaks of CaAlg gel beads at 158°C and GOX at 168°C coalesced and shifted up to 187°C due to the formation of a CaAlg and GOX complex (Fig. 5). The complexation of CaAlg and GOX makes GOX tightly surrounded by CaAlg. As a result, the conformation of GOX would not change when temporary melting of the crystalline region occurs. Since GOX contains 16% polysaccharides in its chemical composition, it is not surprising that CaAlg and chitosan, as polysaccharides, have a stabilizing effect on GOX.

A decrease in enzymatic activity due to enzymatic structure rigidification and steric hindrance is common upon enzyme immobilization, which could significantly reduce the rate of substrate binds onto the catalytic center of the enzyme (47). On the other hand, the diffusion of substrate, e.g. glucose, and reactant oxygen, into the ACMS-GOX takes time. Therefore, a lower H_2O_2 generation rate was seen for ACMS-GOX compared with that of free GOX at short times. For faster reaction, loading GOX near the surface of ACMS is preferred. However, entrapment of the enzyme inside ACMS could protect the enzyme from degradation better.

Cytotoxicity of FR-GOX and ACMS-GOX to Breast Cancer Cells

Both FR-GOX and ACMS-GOX illustrated dose and time dependent cytotoxicity against EMT6 breast cancer cells due to the increased concentration of H_2O_2 with increasing the dose of GOX and exposure time of GOX to cells. The high cytotoxicity of FR-GOX compared to ACMS-GOX at equivalent doses was initially surprising given their similar rates of H_2O_2 generation at longer times (i.e., 3 or 5 h) as shown in Table II. This different potency may be due to the difference in the sites where FR-GOX and ACMS-GOX are generating H_2O_2. The FR-GOX may be more evenly distributed and closer to the cells than ACMS-GOX, as is its generation of H_2O_2, which may impart a faster and more even reaction of ROS with extracellular components and more highly reactive ·OH intracellularly. Our mechanistic study, using various extracellular reactive oxygen metabolite scavengers and intracellular antioxidant enzyme inhibitors and iron chelators, indicated that extracellular H_2O_2 and $^{\cdot}O_2^-$ played a more important role in the cytotoxicity of ACMS-GOX than FR-GOX, and that ·OH is the major ROS accounting for intracellular cytotoxicity (14). As cellular uptake of GOX was not detectable, either upon incubation with FR-GOX or ACMS-GOX and OH has a very short half life (14), it is likely that the intracellular OH was produced inside the cells by H_2O_2 that is generated outside and then diffuses into the cells. This mechanism may also account for the higher potency of FR-GOX.

In Vivo Efficacy in a Murine Solid Tumor Model

Traditional chemotherapy of solid tumors is hampered by the systemic toxicity of therapeutic agents, due to the lack of drug selectivity and the fact that only a small fraction of the drug reaches the tumor tissue in an effective form. To overcome these problems, the present work employed a novel strategy of using ROS-generating enzyme encapsulated in ACMS for intratumoral injection for solid tumor treatment. A significant tumor growth delay was achieved with intratumoral injection of AMCS-GOX in an animal solid tumor model. In contrast, GOX in free form resulted in severe systemic toxicity at equivalent and lower doses. The antitumor activity of GOX is due to its ability to generate H_2O_2 (12), which is demonstrated by a necrotic region in ACMS-GOX treated tumor tissue. No significant weight loss and fur roughing was observed over the treatment period, indicating minimal systemic toxicity was induced by intratumoral injection of ACMS-GOX. At the lower ACMS-GOX dose, no tumor growth delay was seen, which might suggest inadequate H_2O_2 generated by the ACMS-GOX. In solid tumor tissue, the blood flow as well as nutrients, such as oxygen and glucose, may be low (15–18), which, together with a low dose of ACMS-GOX, could lead to a low H_2O_2 generate rate. Since this experiment was only conducted in a limited number of mice, more tests will be undertaken to find the dose dependence and the oxygen and glucose dependence of ACMS-GOX efficacy. Formulation effect on the therapeutic efficacy of ACMS-GOX is also being studied in our laboratory.

CONCLUSIONS

GOX was loaded within the ACMS with higher concentrations near the surface. Electrostatic interaction was a main mechanism of GOX loading into CaAlg gel beads. The formation of the CaAlg-GOX-chitosan complex likely stabilized GOX. GOX retained its integrity after adsorption to CaAlg gel beads and coating of the gel beads with chitosan. ACMS-GOX exhibited cytotoxicity to murine EMT6 breast cancer cells *in vitro* by *in situ* generation of H_2O_2. Intratumorally delivered ACMS-GOX delayed tumor growth in murine solid tumor model with much lower general toxicity than free GOX. The results of this study suggest that the

ACMS-GOX formulation has the potential for the local delivery of therapeutic proteins to treat solid tumors.

ACKNOWLEDGEMENT

This work was supported in part by the Canadian Institutes of Health Research. University of Toronto Open Fellowships and Ben Cohen Fund offered to Q. Liu are also acknowledged. The author would like to thank Dr. T. Chalikian for use of the lyophilizer, Dr. J. Uetrecht for use of the plate reader, Dr. R. Sodhi for XPS experiment and consultation, Mr. H. Huang for DSC analysis, and Mr. B. Calvieri for CLSM imaging analysis. The author would also like to thank Dr. R.Y. Cheung, Dr. H.L. Wong and Mr. A. Shuhendler for their generous help in cell culture work. The authors also thank Mr. Bob Kuba for assistance in animal work.

REFERENCES

1. Kondo N, Nakamura H, Masutani H, Yodoi J. Redox regulation of human thioredoxin network. Antioxid Redox Signal. 2006;8:1881–90.
2. Nicotera TM, Privalle C, Wang TC, Oshimura M, Barrett JC. Differential proliferative responses of Syrian hamster embryo fibroblasts to paraquat-generated superoxide radicals depending on tumor suppressor gene function. Cancer Res. 1994;54:3884–8.
3. Giles GI. The redox regulation of thiol dependent signaling pathways in cancer. Curr Pharm Des. 2006;12:4427–43.
4. Hampton MB, Fadeel B, Orrenius S. Redox regulation of the caspases during apoptosis. Ann N Y Acad Sci. 1998;854:328–35.
5. Visconti R, Grieco D. New insights on oxidative stress in cancer. Curr Opin Drug Discov Devel. 2009;12:240–5.
6. Ravi D, Das KC. Redox-cycling of anthracyclines by thioredoxin system: increased superoxide generation and DNA damage. Cancer Chemother Pharmacol. 2004;54:449–58.
7. Kotamraju S, Konorev EA, Joseph J, Kalyanaraman B. Doxorubicin-induced apoptosis in endothelial cells and cardiomyocytes is ameliorated by nitrone spin traps and ebselen. Role of reactive oxygen and nitrogen species. J Biol Chem. 2000;275:33585–92.
8. Minami T, Adachi M, Kawamura R, Zhang Y, Shinomura Y, Imai K. Sulindac enhances the proteasome inhibitor bortezomib-mediated oxidative stress and anticancer activity. Clin Cancer Res. 2005;11:5248–56.
9. Hagen T, D'Amico G, Quintero M, Palacios-Callender M, Hollis V, Lam F, *et al.* Inhibition of mitochondrial respiration by the anticancer agent 2-methoxyestradiol. Biochem Biophys Res Commun. 2004;322:923–9.
10. Pelicano H, Carney D, Huang P. ROS stress in cancer cells and therapeutic implications. Drug Resist Updat. 2004;7:97–110.
11. Higuchi Y, Shoin S, Matsukawa S. Enhancement of the antitumor effect of glucose oxidase by combined administration of hydrogen peroxide decomposition inhibitors together with an oxygenated fluorocarbon. Jpn J Cancer Res. 1991;82:942–9.
12. Ben-Yoseph Q, Ross BD. Oxidation therapy: the use of a reactive oxygen species-generating enzyme system for tumour treatment. Br J Cancer. 1994;70:1131–5.
13. Liu Q. Enzyme microencapsulation and its application for overcoming multidrug resistance in breast cancer treatment, Ph. D. Dissertation, University of Toronto, Canada 2008.
14. Liu Q, Shuhendler A, Cheng J, Rauth AM, O'Brien PJ, Wu XY. Cytotoxicity and mechanism of action of a new ROS-generating microsphere formulation for circumventing multidrug resistance in breast cancer cells. Breast Cancer Res Treat. 2009; doi:10.1007/s10549-009-0473-3.
15. Folkman J. Tumor angiogenesis: therapeutic implications. N Engl J Med. 1971;285:1182–6.
16. Jain RK. Barriers to drug delivery in solid tumors. Sci Am. 1994;271:58–65.
17. Jain RK. Understanding barriers to drug delivery: high resolution *in vivo* imaging is key. Clin Cancer Res. 1999;5:1605–6.
18. Fang J, Sawa T, Maeda H. Factors and mechanism of "EPR" effect and the enhanced antitumor effects of macromolecular drugs including SMANCS. Adv Exp Med Biol. 2003;519:29–49.
19. Jain RK. Normalization of tumor vasculature: an emerging concept in anitiangiogenic therapy. Science. 2005;307:58–62.
20. Idani H, Matsuoka J, Yasuda T, Kobayashi K, Tanaka N. Intratumoral injection of doxorubicin (Adrimaycin) encapsulated in liposome inhibits tumor growth, prolongs survival time and is not associated with local or systemic side effects. Int J Cancer. 2000;88:645–51.
21. Voulgaris S, Partheni M, Karamouzis M, Dimopoulos P, Papadakis N, Kalofonos HP. Intratumoral doxorubicin in patients with malignant brain gliomas. Am J Clin Oncol. 2002;25:60–4.
22. Liu Z, Ballinger JR, Rauth AM, Bendayan R, Wu XY. Delivery of an anticancer drug and a chemosensitizer to murine breast sarcoma by intratumoral injection of sulfopropyl dextran microspheres. J Pharm Pharmacol. 2003;55:1063–73.
23. Cheung RY, Rauth AM, Wu XY. *In vivo* efficacy and toxicity of intratumorally delivered mitomycin C and its combination with doxorubicin using microsphere formulations. Anti-Cancer Drugs. 2005;16:423–33.
24. Wong HL, Rauth AM, Bendayan R, Wu XY. *In vivo* evaluation of a new polymer-lipid hybrid nanoparticle (PLN) formulation of doxorubicin in a murine solid tumor model. Eur J Pharm Biopharm. 2007;65:300–8.
25. Liu J, Meisner D, Kwong E, Wu XY, Johnston MR. A novel trans-lymphatic drug delivery system: implantable gelatin sponge impregnated with PLGA-paclitaxel microspheres. Biomaterials. 2007;28:3236–44.
26. Liu J, Meisner D, Kwong E, Wu XY, Johnston MR. Trans-lymphatic delivery of paclitaxel by intrapleural placement of gelatin sponge impregnated with PLGA-paclitaxel microspheres effectively controls lymphatic metastasis in an orthotopic lung cancer model. Cancer Res. 2009;69:1174–81.
27. Cheung R, Ying Y, Rauth AM, Marcon N, Wu XY. Biodegradable dextran-based microspheres for delivery of anticancer drug mitomycin C. Biomaterials. 2005;26:5375–85.
28. Liu Q, Rauth AM, Wu XY. Immobilization and bioactivity of glucose oxidase in hydrogel microspheres formulated by an emulsification–internal gelation–adsorption–polyelectrolyte coating method. Int J Pharm. 2007;339:148–56.
29. Fu K, Klibanov AM, Langer R. Protein stability in controlled-release systems. Nat Biotechnol. 2000;18:24–5.
30. Elcin YM, Dixit V, Gitnick G. Extensive *in vivo* angiogenesis following controlled release of human vascular endothelial cell growth factor: implications for tissue engineering and wound healing. Artif Organs. 2001;25:558–65.
31. Peters MC, Isenberg BC, Rowley JA, Mooney DJ. Release from alginate enhances the biological activity of vascular endothelial growth factor. J Biomater Sci Polym Ed. 1998;9:1267–78.
32. Silva CM, Ribeiro AJ, Figueiredo IV, Goncalves AR, Veiga F. Alginate microspheres prepared by internal gelation: development and effect on insulin stability. Int J Pharm. 2006;311:1–10.
33. Hearn E, Neufeld RJ. Poly(methylene co-guanidine) coated alginate as an encapsulation matrix for urease. Proc Biochem. 2000;35:1253–60.
34. Shah Y, Shah D, Patel RB, Trivedi BM. Immobilization of urease in calcium alginate gels. Res Ind. 1995;40:23–7.
35. Betigeri SS, Neau SH. Immobilization of lipase using hydrophilic polymers in the form of hydrogel beads. Biomaterials. 2002;23:3627–36.
36. Hsu SC, Don TM, Chiu WY. Free radical degradation of chitosan with potassium persufate. Polym Degrad Stability. 2002;75:73–83.
37. Roberts GAF, Domszy JG. Determination of the viscometric constants for chitosan. Int J Biol Macromol. 1982;4:374–377.
38. Roberts GAF. Analysis of chitin and chitosan. In: Roberts GAF, editor. Chitin chemistry. London: Macmillan; 1992. p. 95–6.

39. Laemmli UK. Cleavage of structural proteins during the assembly of the head of bacteriophage T4. Nature. 1970;227:680–5.
40. Wang L, Khor E, Lim LY. Chitosan-alginate-$CaCl_2$ system for membrane coat application. J Pharm Sci. 2001;90:1134– 42.
41. Cheung RY, Rauth AM, Ronald P, Bendayan B, Wu XY. Cytotoxicity of microsphere-delivered mitomycin C and its combinations with doxorubicin against breast cancer cells. Eur J Pharm Biopharm. 2006;62:321–31.
42. Tam SK, Dusseault J, Polizu S, Menard M, Halle J, Yahia L. Physicochemical model of alginate–poly-L-lysine microcapsules defined at the micrometric/nanometric scale using ATR-FTIR, XPS, and ToF-SIMS. Biomaterials. 2006;26: 2950–61.
43. Smitha B, Sridhar S, Khan AA. Chitosan-sodium alginate polyion complexes as fuel cell membranes. Eur Polym J. 2005;41:1859–66.
44. Kennamer JE, Usmani AM. DSC analysis of select diagnostic enzymes. J Appl Polym Sci. 1991;42:3073–4.
45. Sarti B, Scandola M. Viscoelastic and thermal properties of collagen/poly (vinyl alcohol) blends. Biomaterials. 1995;16:785–92.
46. Green RJ, Hopkinson I, Jones RAL. Unfolding and intermolecular association in globular proteins adsorbed at interfaces. Langmuir. 1999;15:5102–10.
47. Fersht A. Enzyme Structure and Mechanism. San Francisco: Freeman; 1985.